Langmuir

Article

pubs.acs.org/Langmuir

Fe_3O_4/γ-Fe_2O_3 Nanoparticle Multilayers Deposited by the Langmuir–Blodgett Technique for Gas Sensors Application

S. Capone,[†] M. G. Manera,[†] A. Taurino,[†] P. Siciliano,[†] R. Rella,*[,†] S. Luby,[‡] M. Benkovicova,[‡] P. Siffalovic,[‡] and E. Majkova[‡]

[†]Institute of Microelectronics and Microsystems (C.N.R.-I.M.M.), via Monteroni, Campus Ecotekne, 73100 Lecce, Italy

[‡]Institute of Physics, Slovak Academy of Sciences, Dubravska cesta 9, 845 11 Bratislava, Slovakia

ABSTRACT: Fe_3O_4/γ-Fe_2O_3 nanoparticles (NPs) based thin films were used as active layers in solid state resistive chemical sensors. NPs were synthesized by high temperature solution phase reaction. Sensing NP monolayers (ML) were deposited by Langmuir–Blodgett (LB) techniques onto chemoresistive transduction platforms. The sensing ML were UV treated to remove NP insulating capping. Sensors surface was characterized by scanning electron microscopy (SEM). Systematic gas sensing tests in controlled atmosphere were carried out toward NO_2, CO, and acetone at different concentrations and working temperatures of the sensing layers. The best sensing performance results were obtained for sensors with higher NPs coverage (10 ML), mainly for NO_2 gas showing interesting selectivity toward nitrogen oxides. Electrical properties and conduction mechanisms are discussed.

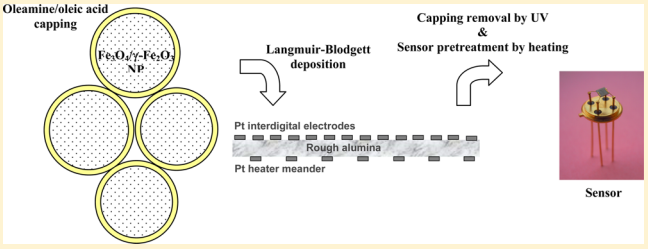

1. INTRODUCTION

Searching for new materials for the development of high performance solid-state gas sensors is one of the main present challenges. Various semiconducting metal oxides thick and thin films and 1-D nanostructures have been prepared and studied as chemoresistive gas sensing materials.[1−3] Among the investigated materials, iron oxides, the Earth's oldest minerals, are the subject of modern interest due to their fascinating magnetic, electric, and dielectric properties.

These properties are largely dependent on the elemental composition, route of materials synthesis, synthesis conditions (sintering conditions, time, etc.), deposition technique, grain size and surface morphology, and heterogeneity in the materials. Fourteen pure phases of iron oxides, i.e., oxides, hydroxides, or oxyhydroxides, are known to date. These are $Fe(OH)_3$, $Fe(OH)_2$, $Fe_5HO_8{\cdot}4H_2O$, Fe_3O_4 (magnetite), FeO, five polymorphs of FeOOH, and four of Fe_2O_3.[5]

Up to now, gas sensing has not been the main application of iron oxides compared to other more extensively explored applications such as magnetic materials and catalysts. Only in recent years there is an increasing interest to study the gas sensing properties of iron oxide-based materials. Some papers investigating gas sensing properties of α- and γ-forms of Fe_2O_3, respectively *hematite* and *maghemite*,[11−17] mixed oxides of Fe and other metals,[18−21] and spinel ferrite,[22−27] are reported in the literature. However, a satisfying knowledge on the gas sensing mechanisms and on chemoresistive transduction of such materials is not established yet. This is mainly linked to some uncertainty concerning the n- and p-type semiconducting properties of iron oxides and transitions between different crystalline phases and polymorphic forms of iron oxides.

Nanoscale is a key factor when studying gas sensing performances of metal oxides. Indeed, in metal oxide semiconductor gas sensors, surface structure of the film and surface-to-volume ratio play a very important role in sensing performance. Nanostructured materials can enhance the performance of gas sensors because of their much higher surface-to-volume ratio as compared to coarse micrograined materials. In addition to the enhanced sensitivity, the sensors can give a quick response as well. In particular, nanostructured gas-sensitive materials based on metal oxides nanoparticles (and contextually on iron oxides NPs) are expected to be good candidates as gas sensors.

Iron oxides can be synthesized by all known wet chemical methods in the forms of nanoparticles (NPs). Important progress has been made for obtaining uniform iron oxides NPs with tunable chemical and magnetic properties. Some of the iron oxide nanoparticles (NPs) synthesis techniques include chemical precipitation, sol–gel, hydrothermal, surfactant-mediated precipitation, emulsion precipitation, microemulsion precipitation, electrodeposition, and microwave-assisted hydrothermal technique.[5−10] The first literature on NPs synthesis methods demonstrated that thermal decomposition of iron oleate complex can produce monodisperse iron oxides NPs in an ultralarge scale; hence, it has become the main approach to high quality iron oxides NPs production.[6,28,29] Since the mechanism leading to the chemical conversions into Fe_3O_4 or Fe_2O_3 is complicated by the multicomponent reactants present in the reaction mixture, a lot of efforts are paid to find the best

Received: November 26, 2013
Revised: January 9, 2014
Published: January 11, 2014

   dx.doi.org/10.1021/la404542u | *Langmuir* 2014, 30, 1190−1197

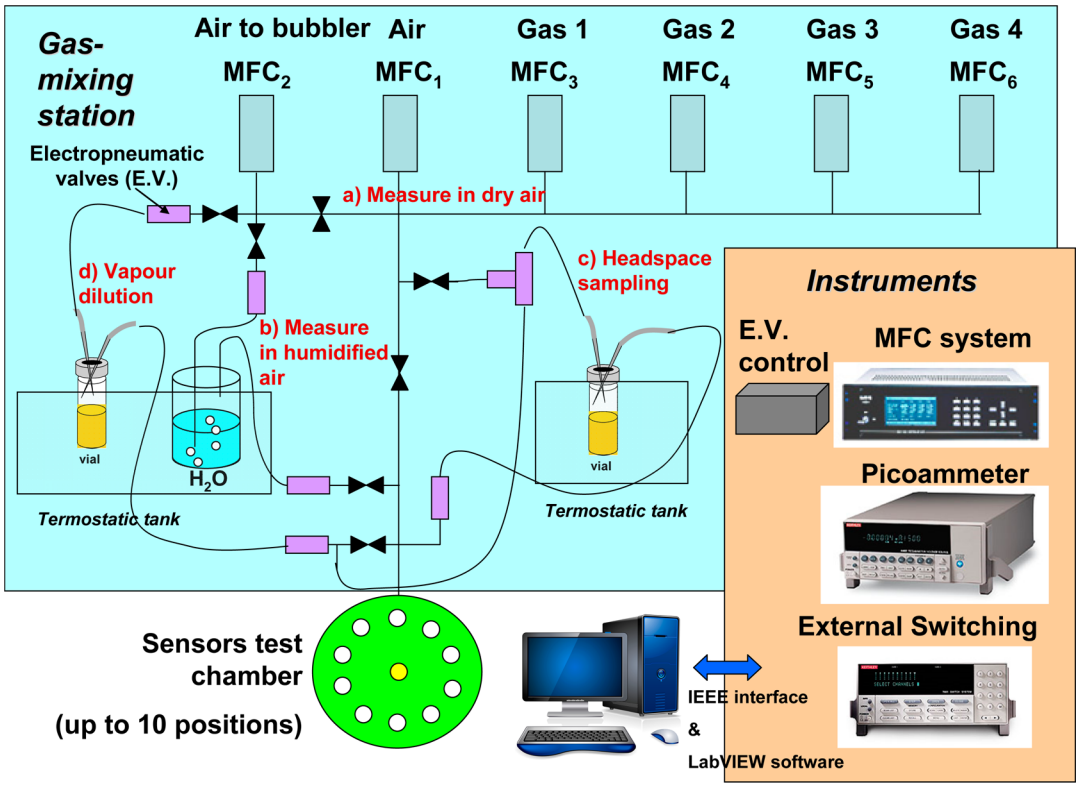

Figure 1. Scheme of the experimental apparatus used for electrical tests performed in a controlled atmosphere.

reliable and simplified recipe that allows a better stoichiometry control and tuning of nanoparticle dimensions.

In this work we introduced a procedure for the synthesis of monodispersed Fe_3O_4/γ-Fe_2O_3 nanoparticles (NPs) by high-temperature decomposition of iron acetylacetonate, $Fe(acac)_3$. We aimed to investigate the gas sensing properties of iron oxide nanoparticles, i.e. Fe_3O_4 (magnetite)/γ-Fe_2O_3 (maghemite), by the resistive transduction principle. Multiple NP layers were deposited by the Langmuir–Blodgett (LB) technique. LB layers were also characterized by XRD and EDS. After surfactant removal, Fe_3O_4/γ-Fe_2O_3 NPs layer-based samples with different numbers of LB monolayers (ML) were calibrated as gas sensors to carbon monoxide (CO), nitrogen dioxides (NO_2), and acetone (C_3H_6O). The influence of the numbers of LB layers and the working temperature on gas sensing performance was considered. It is worth to note that the increase in the number of layers does not means a corresponding increase in the thickness of the film. Surely, at the increasing of the number of layers, the packing density of the NPs is greatly improved, thus improving the whole conductivity of the sensor. In this sense, the study of the influence of the number of LB layers on the gas sensing performance can be considered as the study of the sensing properties of the prepared NPs as a function of their packing density in the active layer.

Morphological characterization by scanning electron microscopy (SEM) was carried out in order to study the uniformity of Fe_3O_4/γ-Fe_2O_3 NPs multilayers covering the rough alumina substrates. SEM observations carried out both before and after gas sensing test at high temperature allowed also arguing about effectiveness of surfactant removal.

2. EXPERIMENTAL SECTION

Monodispersed Fe_3O_4 (magnetite)/γ-Fe_2O_3 (maghemite) nanoparticles (NPs) were synthesized by a high-temperature solution phase of metal acetylacetonates ($Fe(acac)_3$) with 1,2-hexadecanediol, oleic acid, and oleylamine in phenyl ether.[26,27] In a typical synthesis of Fe_3O_4/Fe_2O_3 NPs the reactants (0.353 g of $Fe(acac)_3$, 1.29 g of 1,2-hexadecanediol, 0.847 g of oleic acid, and 0.8025 g of oleylamine) were dissolved in diphenyl ether (20 mL) and magnetically stirred under an argon flow.

The solution was dehydrated at 200 °C for 30 min under an argon atmosphere, next quickly heated up to 265 °C, and held at this temperature for another 30 min. After the reaction, the solution was cooled down to room temperature. After adding a polar solvent (i.e., ethanol), a black particulate product precipitated; in such a way the iron oxides nanoparticles were extracted, centrifuged to remove ethanol, and redispersed into a nonpolar solvent (i.e., toluene).

1,2-Hexadecanediol with two hydroxyl groups acts as a strong reducing agent; both oleic acid and oleylamine act as surfactants. Their above shown weights correspond to the volume ratio 1:1 and similar is their ratio in the capping. Suitable volume oleylamine/diphenyl ether and oleylamine/oleic acid ratios control the particle size. Under the mentioned conditions we get the smallest dispersion of 8% of the nanoparticle size being 6.4 ± 0.5 nm.

Morphological analysis of the as-prepared nanoparticles was carried out by scanning electron microscopy (SEM) and transmission electron microscopy, whereas structural analysis was carried out by grazing incident X-ray (GI XRD) diffraction and by electron diffraction (ED) (XRD-D8 Bruker equipment).[26,27]

Langmuir–Blodgett (LB) films of the as-prepared iron oxides NPs were deposited from the water subphase in the 612 D NIMA trough at the surface pressure of 20 mN/m. With this pressure, which holds provided that there is no free surfactant in the solution, we get a regular nanoparticle monolayer without overlapping areas.

Different samples with 1, 2, 4, and 10 ordered LB monolayers (ML) were deposited by modified Langmuir–Schaefer procedure with the substrate submerged under the water subphase in parallel with its surface. After pumping the water from the trough, the nanoparticle

dx.doi.org/10.1021/la404542u | Langmuir 2014, 30, 1190–1197

monolayers sit down onto the substrate with the transfer ratio approaching 100% in the central part used for sensor preparation. (Some discrepancies may appear on the substrate edges.) Nanoparticles are deposited onto resistive-type transduction platforms, i.e., 3 mm × 3 mm rough alumina substrates equipped with Pt interdigitated electrodes (IDEs) (no. 7 fingers 50 micron spaced) on the front side and Pt heating meander on the back side. Such functional substrates for chemoresistive gas sensors were manufactured by using RF sputtering and standard photolithography technologies in batch fabrication process.

Oleylamine/oleic acid coatings control the stability of the nanoparticles in solution and the dynamics of their self-assembly on surfaces. However, in order to allow electrical conduction through the LB deposited layers of Fe_3O_4/Fe_2O_3 NPs for their direct use as chemoresistive gas sensors, insulating surfactant capping has to be removed from NPs surface. Here, a suitable ultraviolet (UV) irradiation from ozone generating mercury lamp (photon energies 4.6 and 6.7 eV) for 10 min at the flux 2 mW/cm^2 in the ambient of ozone in dry air was used to remove insulating surfactant.[30]

After this pretreatment, the Fe_3O_4/γ-Fe_2O_3 NPs layer-based samples with different numbers of LB monolayers (ML) (i.e., 1−2−4−10 layers) were bounded onto standard electronic TO-39 sockets, and all four were inserted into a steel gastight measuring chamber for electrical calibration as gas sensors (Figure 1). Prior to the gas sensing test, all the samples were thermally stabilized in the test chamber at the working temperature of 500 °C in dry-air flow choosing a conditioning time of 3 days required for the thermodynamic stabilization of the conductivity sensor signal avoiding signal drifts. After this conditioning the gas sensors were exposed to different concentrations of carbon monoxide (CO), nitrogen dioxide (NO_2), and acetone (C_3H_6O) mixed in dry-air at different operating temperatures (200−500 °C). An experimental setup, entirely designed and realized at the Gas Sensor Laboratory of the CNR-IMM in Lecce (Italy), was used, satisfying all the R&D requirements for the testing and calibration of gas sensor heads in controlled environment (flow, concentration, humidity, temperature) and under automated sampling protocols. The gas sensor testing system has the flexibility to carry out measurements toward complex gas mixtures (prepared by a gas-mixing unit regulated by varying the flows through different mass flow controllers (MFCs) connected to synthetic air and gas mixtures bottles) and toward the headspace of samples.[31] The operating temperature of the sensors was varied from 200 to 500 °C at 50 °C stepwise; these temperatures were obtained applying different voltages to the integrated heater of each sensor. The sensors were polarized using a constant voltage of 10 V provided by a programmable power supply (Thunder TTi). The electrical current signals of the sensor array were monitored under several 30 min pulses of exposure to gas concentration, followed by a dry air purge for 90 min. A LabVIEW system design software was suitably designed to control the gas line control system (MKS 674B with four channels) as well as the sampling process and the data acquisition.

The morphology of Fe_3O_4/γ-Fe_2O_3 NPs layer-based gas sensors was investigated by high-resolution scanning electron microscopy, by using an NVISION Zeiss focused ion beam system equipped with a SEM Gemini column and with an Inca Energy 350 X-ACT Oxford energy-dispersive X-ray spectroscopy (EDS) detector.

3. RESULTS AND DISCUSSION

SEM morphological analysis of the as-prepared iron oxides nanoparticles showed that they have spherical shape, with a diameter of 6.4 ± 0.5 nm including a small surfactant capping layer.[26]

The GIXRD spectra of the Fe−O system (Figure 2a) correspond to either Fe_3O_4 (magnetite, cubic fcc) or γ-Fe_2O_3 (maghemite, cubic, primitive cell). From the peaks at larger diffraction angles γ-Fe_2O_3 composition is preferred.[27] Moreover, under the aging/heating in air or UV irradiation Fe_3O_4 is oxidized to Fe_2O_3.[32] We have confirmed this oxidation by X-ray

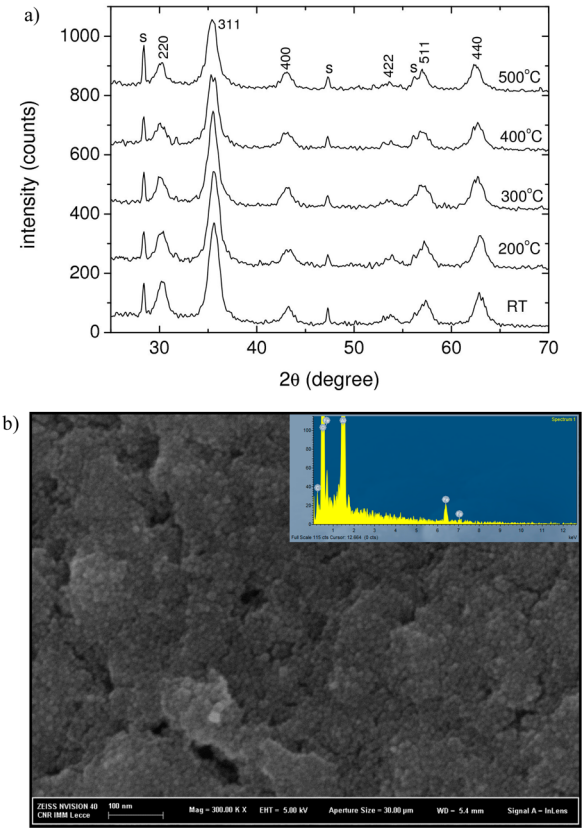

Figure 2. (a) GIXRD studies of vacuum isochronal annealing of Fe_2O_3 NPs. (b) SEM image of the same sensor at high magnification; EDS microanalysis in the inset.

absorption near-edge structure measurement (XANES) at the Fe K edge (7112 eV) using the resemblance with the postedge region of Fe_2O_3 powder (not shown here).

Thermal stability of our NPs was studied by GIXRD on the oxidized Si substrates at the isochronal heating in dry vacuum of 10^{-6} Pa at 200 °C, etc., up to 500 °C, 30 min at each temperature (500 °C is the highest temperature of sensors in many applications). Results for Fe_2O_3 NPs are shown in Figure 2a. NPs were chemically stable up to 500 °C, and the coalescence or neck formation was not observed. Details of these characterizations as well as magnetic characterization are reported elsewhere.[26,27]

The Fe_3O_4/γ-Fe_2O_3 NPs layer-based sensors (1−2−4−10 ML) were characterized by SEM after the sensing tests. All samples exhibited continuous nanoparticle coverage, whose density increases with the number of the monolayers. As an example, in Figure 2 we reported the SEM analysis of the Fe_3O_4/γ-Fe_2O_3 NPs-based sensor with 10 ML. The coverage follows the roughness of the alumina substrates. The EDS microanalysis (inset of Figure 2b) clearly reveals the presence of signals coming from the NPs-based sensors, i.e. Fe and O, whereas Al and C derive from the alumina substrate and from external contamination, respectively.

SEM analyses performed on the sensors before their gas-sensing tests did not allow obtaining significant data at high resolution because of the severe charging effects related to the insulating nature of the samples. This result, even though unimportant from the morphological characterization point of view, allowed us deriving interesting information on the oleylamine/oleic acid capping removal process of the NPs

dx.doi.org/10.1021/la404542u | Langmuir 2014, 30, 1190−1197

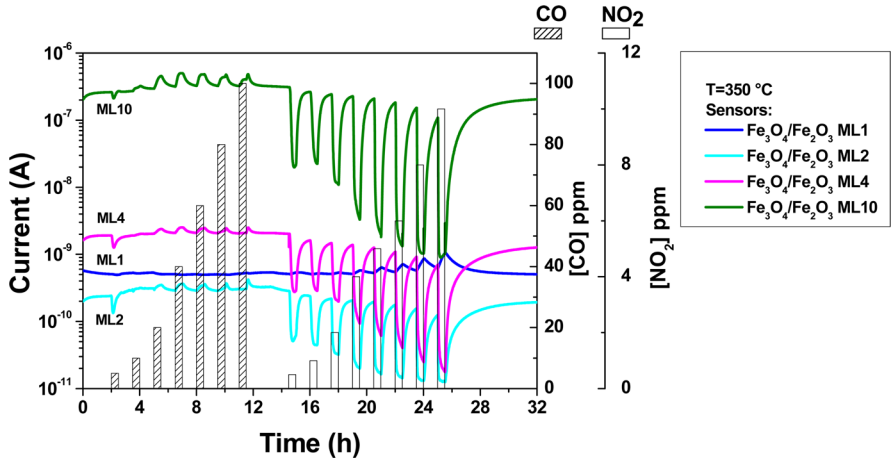

Figure 3. Dynamic responses (electrical current vs time) of the set of Fe_3O_4/Fe_2O_3 NPs-based sensors at a programmed protocol of gas sensing tests toward CO and NO_2 at the best working temperature of 350 °C. Sensors polarization was 10 V.

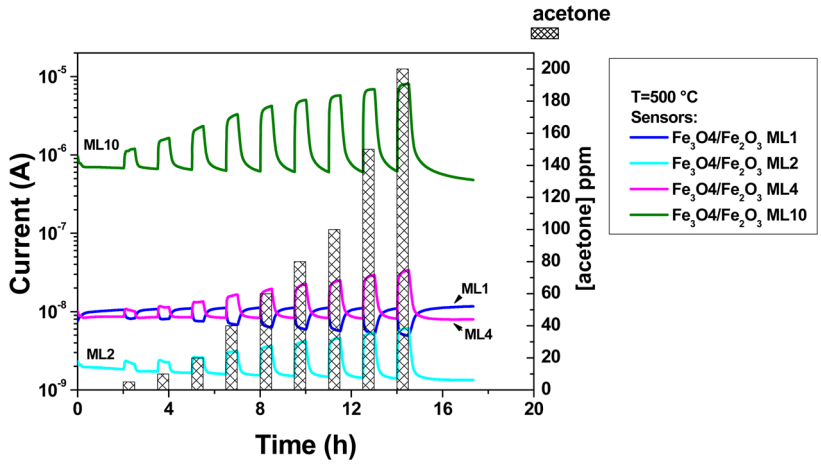

Figure 4. Dynamic responses (electrical current vs time) of the set of Fe_3O_4/Fe_2O_3 NPs-based sensors at a programmed protocol of gas sensing tests toward acetone at the best working temperature of 500 °C. Sensors polarization was 10 V.

before their characterization as sensors. As a matter of fact, the different behavior of the NPs films during the SEM analyses, before the sensing tests, revealed a not complete removal of NPs capping material, giving rise to an evident electrical charging, due to the interaction between the SEM electron beam and the nanoparticles insulating coverage by surfactant agents. No evidence of organic surfactant capping was observed by EDS microanalysis, within the instrumental detection limit. However, this can be attributed to the very thin thickness of oleylamine/oleic acid coverage, remaining after the UV/ozone treatment. In the literature various methods were applied to remove the oleylamine surfactant from colloidal nanoparticles, which included thermal annealing, acetic acid washing, and UV-ozone irradiation.[30] In our study, the used UV/ozone pretreatment of Fe_3O_4/γ-Fe_2O_3 NPs samples is not sufficient to completely remove the surfactant capping consisting of oleylamine/oleic acid, whereas it seems necessary an extended period at high temperature to slowly eliminate the insulating capping from the NPs. A reduction in the size of the NPs of about 1.6 nm can be evidenced after this annealing due to the complete removal of the organic surfactant.

This observations also agreed with the initial high resistance of all the γ-Fe_3O_4/Fe_2O_3 NPs sensors (>GΩ) at the beginning of the gas sensing tests; a settling-down period of 3 days at 500 °C was hence found necessary to both remove any capping residues and stabilize morphology and electrical properties of the samples in operative sensor conditions (i.e., in dry air). After a stabilizing treatment in the gas measuring chamber, gas sensing tests under a systematic protocol, at different working temperatures and different gas concentrations, gave the following results.

In Figure 3, we reported the dynamic responses of the set of Fe_3O_4/γ-Fe_2O_3 NPs-based sensors at a programmed protocol of gas sensing tests toward different concentrations of CO (5−10−20−40−60−80−100 ppm in dry air) and NO_2 (0.5−1−2−4−5−6−8−10 ppm in dry air) at the maximum response working temperature of 350 °C. Sensor responses were calculated as I_{air}/I_{NO_2} and I_{CO}/I_{air}, respectively, where I_{air}, I_{NO_2}, and I_{CO} are the values of electrical current in air, NO_2, and CO, respectively. On the other side, Figure 4 shows the gas sensing tests toward C_3H_6O (acetone: 5−10−20−40−60−80−100−150−200 ppm in dry air) at the maximum response working temperature of 500 °C. It can be observed that the Fe_3O_4/γ-Fe_2O_3 NPs-based sensors with 2, 4, and 10 monolayers (ML) showed a high decrease of conductivity (i.e., electrical current under constant polarization) under exposure to oxidizing gas as NO_2 and a very low but appreciable increase of conductivity under reducing gases as CO and acetone, respectively; this is

dx.doi.org/10.1021/la404542u | Langmuir 2014, 30, 1190−1197

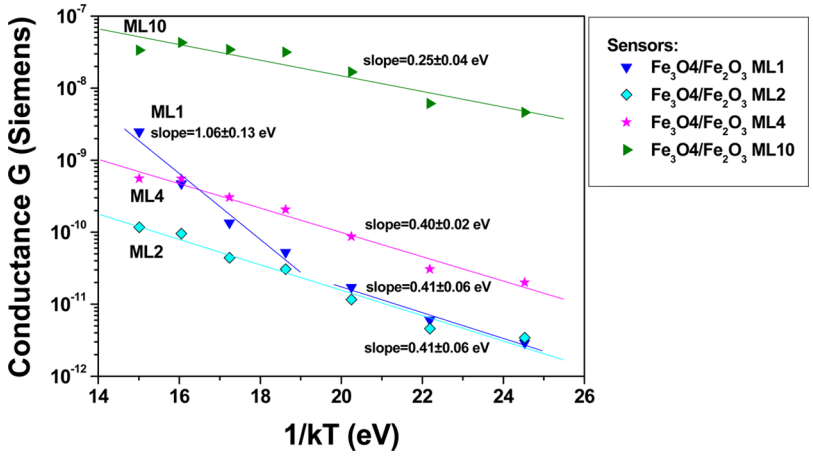

Figure 5. Arrhenius plot (i.e., conductance vs $1/kT$) for all the Fe_3O_4/Fe_2O_3 NPs-based sensors.

ascribed to an n-type semiconducting behavior of the sensing materials (n-type response to gases). Surprisingly, Fe_3O_4/γ-Fe_2O_3 NPs-based sensor with 1 ML showed a p-type response to gases; its conductivity increases under exposure to NO_2 (although the relative conductivity variation is much lower than the correspondently n-type responses of the other samples), and it decreases under exposure to acetone, whereas a minimum decrease was registered under CO exposure.

For understanding such phenomena we can refer to what is known about the electrical and conduction properties of iron oxides, which are besides closed linked to their structural and magnetic properties.

Fe_3O_4 (magnetite) arranged in a cubic close-packed lattice. Both FeO and γ-Fe_2O_3 have a similar cubic close-packed array of oxide ions, and this accounts for the ready interchangeability between the three compounds on oxidation and reduction as these reactions entail a relatively small change to the overall structure. This explains also that both phases Fe_3O_4 and γ-Fe_2O_3 were found in the prepared nanoparticles. However, it should be considered that the relative percentage of Fe_3O_4 and γ-Fe_2O_3 in our Fe−O systems of iron nanoparticles can depend on the oxidation $Fe_3O_4 \rightarrow Fe_2O_3$ due to the thermal treatment at the sensor working temperature during the gas-sensing measurements in dry air. Moreover, γ-Fe_2O_3 is metastable and at high temperatures (starting over 450 °C) gradually converts to α-Fe_2O_3 phase (*hematite*) that has the rhombohedral, corundum (α-Al_2O_3) structure.[4,21,22] However, it is worth to observe that change of phase does not influence the sensing properties of the investigated sensor. In fact, prior to the gas sensing test, all the samples were thermally treated at the highest temperature (500 °C) in dry air for many days. After this conditioning step in the carrier gas, the sensing experiment at different concentrations of analytes and at different lower temperatures has been carried out. So, if a change in phase is occurred, it does happen during the sensing experiment.

The Fe_3O_4 is known to be a half-metal that follows a transition to insulator for $T < T_V$ (Verwey transiton at $T = 122$ K), even if this is still controversial. A half-metal is any substance that acts as a conductor to electrons of one spin orientation but as an insulator or semiconductor to those of the opposite orientation. In a band energy model of Fe_3O_4, it occurs that the majority spin-down band and the minority spin-up band are separated. Moreover, the five degenerate d-electron levels of Fe cations are further splitted into three degenerate t_{2g} levels and two e_g levels. For both Fe^{2+} and Fe^{3+} cations, the five electrons occupy the majority t_{2g} and e_g levels; the extra electron of the Fe^{2+} occupies the minority t_{2g} band, which is the only band (partially filled) located at the Fermi level E_F, giving rise to half-metallic behavior of magnetite (i.e., its electronic density of states is spin polarized at the Fermi level E_F, and the conductivity is dominated by these spin-polarized charge carriers). In such a way, the conduction of magnetite is attributed to a continuous hopping (thermally activated fast electron hopping) of these extra electrons from Fe^{2+} to Fe^{3+} cations randomly distributed over the crystallographic B-octahedral sites of the inverse spinel structure. The fact that other spinel ferrites such as $CoFe_2O_4$, $NiFe_2O_4$, and $MnFe_2O_4$ with only Fe^{3+} cations in B_{oct} sites are insulators (really semiconductors) strongly supports this explanation. On the other hand, the majority spin-up band is separated from conduction band above by an energy gap, giving rise to semiconduction (1.4 eV band gap). Magnetite Fe_3O_4 has hence really half-metallic behavior with a semiconducting majority-spin channel and a conductive minority-spin channel, resulting in a 100% spin polarization at E_F.[33,34]

On the contrary, maghemite γ-Fe_2O_3 is an n-type semiconductor with a band gap of 2.03 eV. It is also ferromagnetic although ultrafine particles smaller than 10 nm are superparamagnetic.[4] At high temperature (almost above 450 °C) maghemite γ-Fe_2O_3 can gradually transform into hematite α-Fe_2O_3 that is also n-type semiconductor with a band gap of 2.2 eV. α-Fe_2O_3 is antiferromagnetic below ∼260 K (Morin transition temperature) and exhibits weak ferromagnetism between 260 K and the Néel temperature, 950 K.[4]

In reference to this literature scenario, we have to consider that nanoparticles tested in this work are really a combination of both phases Fe_3O_4 and γ-Fe_2O_3 and that the temperature treatment of our Fe_3O_4/γ-Fe_2O_3 samples under sensor working conditions could have modified the structural composition of the nanoparticles, favoring an evolution $Fe_3O_4 \rightarrow \gamma$-$Fe_2O_3 \rightarrow \alpha$-$Fe_2O_3$. The inverse response to NO_2 (extracting electrons from the material) and acetone (releasing electrons to the material) could be tentatively attributed to an enhancement (respectively reduction) of half-metallic conduction. The extraction of electron by NO_2 could let the filled semiconducting majority spin sub-band transforming into a partially filled sub-band with an additional half-metallic contribution to conduction, whereas the injection of electron by acetone could fill the minority spin sub-band, hence reducing the electron hopping mechanism between available free sites.

dx.doi.org/10.1021/la404542u | *Langmuir* 2014, 30, 1190−1197

There are also other questions to be considered. The electrical conduction in semiconductors can be due not only to impurities/dopants but also to intrinsic nonstoichiometry. In general, oxygen anions (O^{2-}) vacancies inside the metal oxide leave behind extra electrons and produce an n-type semiconduction; metal cations (M^{n+}) deficiencies leave behind extra holes and produce a p-type conduction. Nonstoichiometry is pervasive for transition metal oxides, especially when the metal is not in its highest oxidation state. This is what can happen in γ-Fe_2O_3 and α-Fe_2O_3 when a kind of nonstoichiometry (n- or p-) defect prevails, under particular conditions (due to preparation process, treatment in oxidizing or reducing atmosphere, etc.).

Other authors have however observed an inversion from n-type to p-type semiconduction in α-Fe_2O_3, and they attributed it to a strong adsorption of ambient oxygen species that results in the formation of an inversion layer near the surface, where the Fermi level is below the intrinsic level. Holes become the majority carriers, which result in a surface p-type conductivity inside an n-type semiconductor.[14−17] We have no evidence of which of the analyzed possible mechanisms is responsible for the experimented electrical behavior of our Fe_3O_4/γ-Fe_2O_3-based NPs sensors. We can only underline that this effect was already registered by other authors and that in our case it occurs only for the sample with 1 ML.

Further results obtained with the Fe_3O_4/γ-Fe_2O_3-based NPs sensors with 2−4−10 ML demonstrate that the electrical conductance G of the samples increases with increasing the numbers of deposited LB monolayers ($G_{ML2} < G_{ML4} < G_{ML10}$) at all the working temperatures. Figure 5 shows the Arrhenius plot (i.e., conductance vs $1/kT$) for all the sensors Fe_3O_4/Fe_2O_3. It results that the Fe_3O_4/γ-Fe_2O_3-based NPs sensors with 2−4−10 ML have low activation energies (∼0.25−0.41 eV), whereas the sensors with 1 ML have a bit higher activation energy (∼1.06 eV) at high T and a lower activation energy (∼0.41 eV) at low T. The low values of activation energies lead us to suppose that in this situation conduction proceeds only by phonon-assisted tunnelling, or "hopping", between localized electron states. This hopping is a thermally activated process in which electron tunneling occurs simultaneously with the absorption or emission of a phonon whose energy accounts for the difference between the initial and final electron states. So, if we consider that electron transport takes place by a combination of percolation through a network of sites and thermal accessibility of energy states,[35,36] we have that at activated temperature, as the number of layers increases also the number of percolating/conduction routes increases, thus increasing conduction.

Figure 6 shows the gas response curves of the Fe_3O_4/Fe_2O_3 with 2−4−10 ML to the considered analytes: NO_2, CO, and acetone; the gas response is defined as the fractional I_{air}/I_{NO_2} or I_{CO}/I_{air} and $I_{acetone}/I_{air}$ ratio. All the sensors showed higher sensing properties to NO_2 as compared to CO and acetone. At $T \leq 400$ °C the responses of Fe_3O_4/Fe_2O_3 ML10-based sensor toward NO_2 are 2 orders of magnitude higher than the responses of sensors with ML2 and ML4, whereas at $T > 400$ °C Fe_3O_4/Fe_2O_3 ML2-, ML4-, and ML10-based sensors show comparable responses within the experimental error (calculated on the basis of five equivalent samples). Moreover, at increasing the numbers of layers there is a decreasing of the optimal working temperature; Fe_3O_4/Fe_2O_3 ML10-based sensor has a response curve with a maximum at T = 350−400 °C.

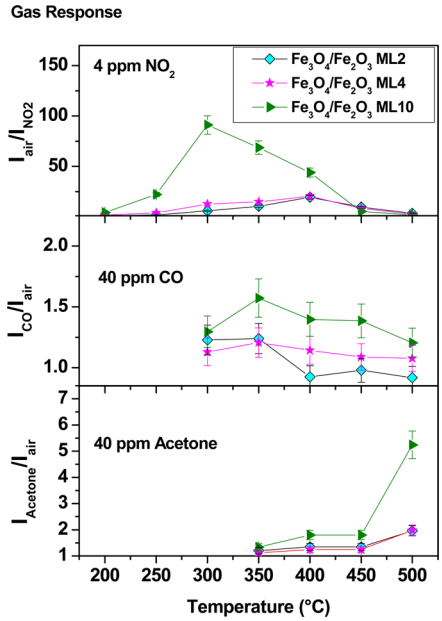

Figure 6. Gas response curves of the 2−4−10 ML Fe_3O_4/Fe_2O_3 NPs-based sensors (i.e., fractional I_{air}/I_{NO_2} or I_{CO}/I_{air} and $I_{acetone}/I_{air}$) vs working temperature.

This behavior is currently explained taking into account that the oxide surface is populated by a variety of physisorbed and chemisorbed molecules, in particular H_2O, OH^-, O_2, O_2^-, and O^-, where O^- and O_2^- are likely to predominate. The presence of these species modulates the electrical behavior of the active layer in the presence of the oxidizing or reducing gases. At the temperature of the active layer of about 300−400 °C the species O_2^- and O^- are dominant in the sensing mechanism. At these temperatures NO can be absorbed or interact with the oxygen adsorbed onto the sensing layer according to the reactions

$$NO_{2gas} + e^- \rightarrow NO_2^-$$

$$NO_{2gas} + O_2^- + 2e^- \rightarrow NO_2^- + 2O^-$$

These reactions reduce the electron concentration near the surface, and consequently the resistance of the layer increases. Moreover, NO_2 ions are desorbed as NO_2 gas flow is stopped and consequently a recovery of the initial condition takes place.

The gas responses toward carbon monoxide are very low, comparable with values found in a *previous* experimental work.[26] The Fe_3O_4/Fe_2O_3 ML10-based sensor has the better sensitivity with an optimum working temperature again at T = 350−400 °C. The gas response toward acetone is higher than that to CO. Acetone was detected only at high temperature (≥350 °C); at $T \sim 500$ °C the sensor can work properly.

The increase of the current I in the presence of reducing gases such as CO and acetone may be explained by the reaction between the analyte gas and chemisorbed oxygen on the surface of the active layer (let us consider CO as an example):

$$2CO_{gas} + {O_2^-}_{ads} \rightarrow 2CO_{gas} + e^-$$

In fact, this reaction reduces the band bending of the intergranular depletion layers and, subsequently, leads to an increase of the sensor current.

Calibration curves for NO_2 of the Fe_3O_4/Fe_2O_3 NPs-based gas sensors with 1−2−4−10 ML at the working temperature of

dx.doi.org/10.1021/la404542u | *Langmuir* 2014, 30, 1190−1197

350 °C are reported in Figure 7. In the concentration range with a linear dependence in the log−log graph, the sensitivities

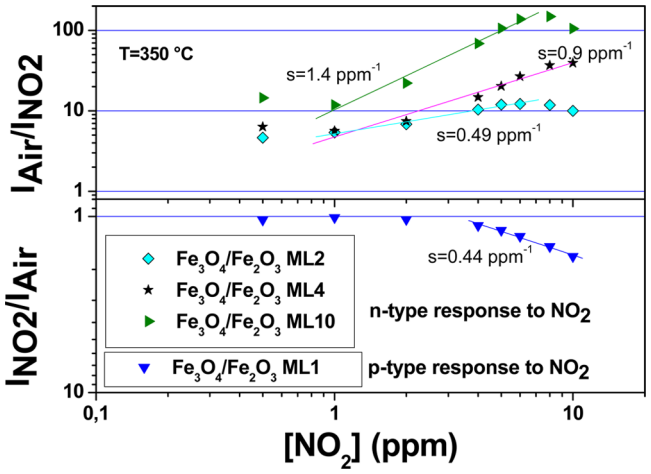

Figure 7. Calibration curves for NO_2 of the 1−2−4−10 ML Fe_3O_4/Fe_2O_3 NPs-based gas sensors at the working temperature of 350 °C.

of the sensors were calculated; the sensitivity increases with increasing the numbers of ML. The sensor ML10 has the higher sensitivity s (s = 1.4 ppm^{-1}), then the sensor ML4 follows with s = 0.9 ppm^{-1}, and then the sensor ML2 with s = 0.49 ppm^{-1}. All the sensors showed a trend to saturation over 8 ppm of NO_2. The singular behavior of sensor with ML1 with a p-type response to NO_2 showed a sensitivity s = 0.44 ppm^{-1}.

Calibration curves for acetone of the Fe_3O_4/Fe_2O_3 NPs-based gas sensors with 1−2−4−10 ML at the working temperature of 500 °C are reported in Figure 8. Here linear

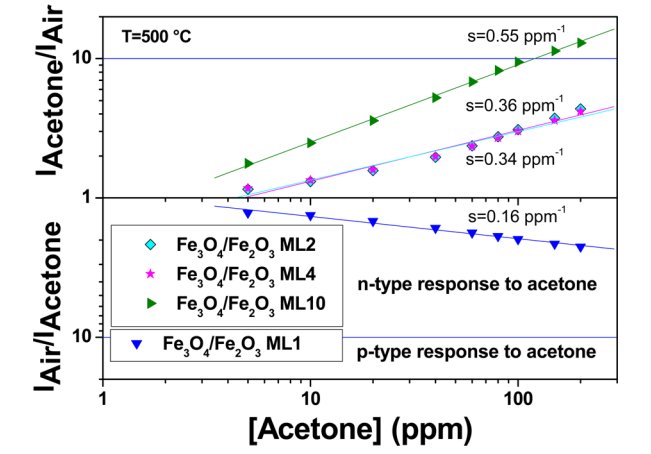

Figure 8. Calibration curves for acetone of the 1−2−4−10 ML Fe_3O_4/Fe_2O_3 NPs-based gas sensors at the working temperature of 500 °C.

dependences were found in all the analyzed concentration range. Also for acetone, the sensitivity increases with increasing the numbers of ML; in particular, s_{ML1} = 0.16 ppm^{-1} < s_{ML2} = 0.34 ppm^{-1} < s_{ML1} = 0.36 ppm^{-1} < s_{ML10} = 0.55 ppm^{-1}. The calibration curves for CO are not reported since the response for this gas is too low.

4. CONCLUSIONS

In summary, we prepared organic-capped Fe_3O_4/γ-Fe_2O_3 nanoparticles of 6.4 ± 0.5 nm diameter by a high-temperature solution phase reaction of metal acetylacetonates. The nanoparticles have spherical shape and well-developed crystalline structures. Monolayers of nanoparticles were deposited by the Langmuir−Blodgett technique onto miniaturized alumina substrates equipped with interdigitated electrodes and heating meander, and the gas sensing properties of the as-prepared chemoresistive gas sensor samples were investigated. Oxidizing (NO_2) and reducing (CO and acetone) gases were considered as analytes. All the sensors showed an n-type response to gases, except the sensors with 1 ML that showed a p-type response. The results were discussed and related to electrical properties of iron oxides and the conduction transport in nanostructured films. The conductance increases with increasing number of ML; also, the NPs coverage increases with number of ML as shown by SEM observation of the sensor surfaces. Fe_3O_4/γ-Fe_2O_3 NPs ML10-based samples gave the higher performance in terms of sensor response and sensitivity as compared to the other samples with lower numbers of ML. Generally the results to NO_2 are better as compared to CO and acetone.

AUTHOR INFORMATION

Corresponding Author

*E-mail roberto.rella@le.imm.cnr.it (R.R.).

Notes

The authors declare no competing financial interest.

ACKNOWLEDGMENTS

We wish to thank Dr. Matej Jergel for GIXRD measurements and useful discussion. We acknowledge the support by Slovak Grant Agency VEGA, grant 2/0162/12, and by the common project of CNR/SAS 2013−2015.

REFERENCES

(1) Wang, C.; Yin, L.; Zhang, L.; Xiang, D.; Gao, R. Review - Metal Oxide Gas Sensors: Sensitivity and Influencing Factors. *Sensors* **2010**, *10*, 2088−2106.

(2) Di Francia, G.; Alfano, B.; La Ferrara, V. Review Article - Conductometric Gas Nanosensors. *J. Sens.* **2009**, Article ID 659275, 18 pp.

(3) Arafat, M. M.; Dinan, B.; Akbar, S. A.; Haseeb, A. S. M. A. Gas Sensors Based on One Dimensional Nanostructured Metal-Oxides: A Review. *Sensors* **2012**, *12*, 7207−7258.

(4) Cornell, R. M.; Schwertmann, U. *The Iron Oxides: Structure, Properties, Reactions, Occurrences and Uses*; Wiley-VCH Verlag GmbH & Co. KGaA: Weinheim, 2003.

(5) Mohapatra, M.; Anand, S. Synthesis and Applications of Nano-Structured Iron Oxides/Hydroxides − A Review. *Int. J. Eng., Sci. Technol.* **2010**, *2* (No. 8), 127−146.

(6) Xu, Z.; Shen, C.; Hou, Y.; Gao, H.; Sun, S. Oleylamine as Both Reducing Agent and Stabilizer in a Facile Synthesis of Magnetite Nanoparticles. *Chem. Mater.* **2009**, *21*, 1778−1780.

(7) Wu, W.; He, Q.; Jiang, C. Magnetic Iron Oxide Nanoparticles: Synthesis and Surface Functionalization Strategies. *Nanoscale Res. Lett.* **2008**, *3*, 397−415.

(8) Wahajuddin, S. A. Superparamagnetic Iron Oxide Nanoparticles: Magnetic Nanoplatforms As Drug Carriers. *Int. J. Nanomed.* **2012**, *7*, 3445−3471.

(9) Pascu, O.; Carenza, E.; Gich, M.; Estradé, S.; Peiró, F.; Herranz, G.; Roig, A. Surface Reactivity of Iron Oxide Nanoparticles by Microwave-Assisted Synthesis; Comparison with the Thermal Decomposition Route. *J. Phys. Chem. C* **2012**, *116* (No.28), 15108−15116.

(10) Yue, J.; Jiang, X.; Valentino Kaneti, Y.; Yu, A. Experimental and Theoretical Study of Low-Dimensional Iron Oxide Nanostructures. In

Smart Nanoparticles Technology; Hashim, A., Ed.; 2012; Chapter 6, pp 119−145.
(11) Wang, G.; Gou, X.; Horvat, J.; Park, J. Facile Synthesis and Characterization of Iron Oxide Semiconductor Nanowires for Gas Sensing Application. *J. Phys. Chem. C* **2008**, *112*, 15220−15225.
(12) Pawar, N. K.; Kajale, D. D.; Patil, G. E.; Wagh, V. G.; Gaikwad, V. B.; Deore, M. K.; Jain, G. H. Nanostructured Fe_2O_3 Thick Film as an Ethanol Sensor. *Int. J. Smart Sens. Intell. Syst.* **2012**, *5* (No. 2), 441−457.
(13) Lim, I.-S.; Jang, G.-E.; Kim, C.; Yoon, D. H. Fabrication and Gas Sensing Characteristics of Pure and Pt-Doped γ-Fe_2O_3 Thin Films. *Sens. Actuators, B* **2001**, *77*, 215−220.
(14) Gurlo, A.; Sahm, M.; Oprea, A.; Barsan, N.; Weimar, U. A p- to n-Transition on α-Fe_2O_3-Based Thick Film Sensors Studied by Conductance and Work Function Change Measurements. *Sens. Actuators, B* **2004**, *102*, 291−298.
(15) Gurlo, A.; Barsan, N.; Oprea, A.; Sahm, M.; Sahm, T.; Weimar, U. An n- to p-Type Conductivity Transition Induced by Oxygen Adsorption on α-Fe_2O_3. *Appl. Phys. Lett.* **2004**, *85*, 2280−2282.
(16) Lee, Y.-C.; Chueh, Y. L.; Hsieh, C.-H.; Chang, M.-T.; Chou, L.-J.; Wang, Z. L.; Lan, Y.-W.; Chen, C.-D.; Kurata, H.; Isoda, S. p-Type α-Fe_2O_3 Nanowires and Their n-Type Transition in a Reductive Ambient. *Small* **2007**, *3* (No.8), 1356−1361.
(17) Hao, Q.; Li, L.; Yin, X.; Liu, S.; Li, Q.; Wang, T. Anomalous Conductivity-Type Transition Sensing Behaviours of n-Type Porous α-Fe_2O_3 Nanostructures toward H_2S. *Mater. Sci. Eng., B* **2001**, *176*, 600−605.
(18) Neri, G.; Bonavita, A.; Rizzo, G.; Galvagno, S.; Capone, S.; Siciliano, P. Methanol Gas-Sensing Properties of CeO_2−Fe_2O_3 Thin Films. *Sens. Actuators, B* **2006**, *114*, 687−695.
(19) Mohammadi, M. R.; Fray, D. J. Low Temperature Nanocrystalline TiO_2−Fe_2O_3 Mixed Oxide by a Particulate Sol−Gel Route: Physical and Sensing Characteristics. *Physica E* **2012**, *46*, 43−51.
(20) Comini, E.; Pandolfi, L.; Kaciulis, S.; Faglia, G.; Sberveglieri, G. Correlation between Atomic Composition and Gas Sensing Properties in Tungsten-Iron Oxide Thin Films. *Sens. Actuators, B* **2007**, *127* (1), 22−28.
(21) Ivanovskaya, M. I.; Kotsikau, D. A.; Taurino, A.; Siciliano, P. Structural Distinctions of Fe_2O_3-In_2O_3 Composites Obtained by Various Sol-Gel Procedures, and Their Gas-Sensing Features. *Sens. Actuators, B* **2007**, *124* (1), 133−142.
(22) Gadkari, A. B.; Shinde, T. J.; Vasambekar, P. N. Ferrite Gas Sensors. *IEEE Sens. J.* **2011**, *11* (No. 4), 849−861.
(23) Leroux, Ch.; Bendahan, M.; Ajroudi, L.; Madigou, V.; Mliki, N.; Cobalt Ferrite, a New Gas Sensing Material. *Proc. IMCS* **2012** (The 14th International Meeting on Chemical Sensors), 119−1121.
(24) Rahman, M. M.; Khan, S. B.; Faisal, M.; Asiri, A. M.; Alamry, K. A. Highly Sensitive Formaldehyde Chemical Sensor Based on Hydrothermally Prepared Spinel $ZnFe_2O_4$ Nanorods. *Sens. Actuators, B* **2012**, *171−172*, 932−937.
(25) Xiangfeng, C.; Dongli, J.; Yu, G.; Chenmou, Z. Ethanol Gas Sensor Based on $CoFe_2O_4$ Nano-crystallites Prepared by Hydrothermal Method. *Sens. Actuators, B* **2006**, *120*, 177−181.
(26) Luby, S.; Chitu, L.; Jergel, M.; Majkova, E.; Siffalovic, P.; Caricato, A. P.; Luches, A.; Martino, M.; Rella, R.; Manera, M. G. Oxide Nanoparticles Arrays for Sensors of CO and NO_2 Gases. *Vacuum* **2012**, *86*, 590−593.
(27) Chitu, L.; Jergel, M.; Majkova, E.; Luby, S.; Capek, I.; Satka, A.; Ivan, J.; Kovac, J.; Timko, M. Structure and Magnetic Properties of $CoFe_2O_4$ and Fe_3O_4 Nanoparticles. *Mater. Sci. Eng., C* **2007**, *27*, 1415−1417.
(28) Park, J.; An, K.; Hwang, Y.; Park, J. G.; Noh, H. J.; Kim, J. Y.; Park, J. H.; Hwang, N. M.; Hyeon, T. Ultra-Large-Scale Syntheses of Monodisperse Nanocrystals. *Nat. Mater.* **2004**, *3* (No. 12), 891−895.
(29) Sun, S.; Zeng, Z. H.; Robinson, D. B.; Raoux, S.; Rice, P. M.; Wang, S. X.; Guanxiong, G. Monodisperse MFe_2O_4 (M = Fe, Co, Mn) Nanoparticles. *J. Am. Chem. Soc.* **2004**, *126*, 273−279.
(30) Li, D. G.; Wang, C.; Tripkovic, D.; Sun, S. H.; Markovic, N. M.; Stamenkovic, V. R. Surfactant Removal for Colloidal Nanoparticles from Solution Synthesis: The Effect on Catalytic Performance. *ACS Catal.* **2012**, *2* (Issue 7), 1358−1362.
(31) Capone, S.; Tufariello, M.; Francioso, L.; Montagna, G.; Casino, F.; Leone, A.; Siciliano, P. Aroma Analysis by GC/MS and Electronic Nose Dedicated to Negroamaro and Primitivo Typical Italian Apulian Wines. *Sens. Actuators, B* **2013**, *179*, 259−269.
(32) Kiyomura, T.; Maruo, Y.; Gomi, M. Electrical Properties of MgO Insulating Layers in Spin-Dependent Tunneling Junctions Using Fe_3O_4. *J. Appl. Phys.* **2000**, *88*, 4768−4771.
(33) Wang, W.; Mariot, J.-M.; Richter, M. C.; Heckmann, O.; Ndiaye, W.; De Padova, P.; Taleb-Ibrahimi, A.; Le Fevre, P.; Bertran, F.; Bondino, F.; Magnano, E.; Krempasky, J.; Blaha, P.; Cacho, C.; Parmigiani, F.; Hricovini, K. Fe t_{2g} Band Dispersion and Spin Polarization in Thin Films of Fe_3O_4(001)/MgO(001): Half-Metallicity of Magnetite Revisited. *Phys. Rev. B* **2013**, *87*, 085118.
(34) Fursina, A. Investigation of Electrically Driven Transition in Magnetite Fe_3O_4 Nanostructures. Ph.D. Thesis, Rice University, 2010.
(35) Skinner, B.; Chen, T.; Shklovskii, B. I. Theory of Hopping Conduction in Arrays of Doped Semiconductor Nanocrystals. *Phys. Rev. B* **2012**, *85*, 205316.
(36) Anta, J. A. Electron Transport in Nanostructures Metal-Oxide Semiconductors. *Curr. Opin. Colloid Interface Sci.* **2012**, *17*, 124−131.